Title

Long-term Evolution and Remodeling of Soft Drusen in Rhesus Macaques

Journal

Investigative Ophthalmology & Visual Science, 61(2)

ISSN

0146-0404

Authors

Yiu, Glenn
Chung, Sook Hyun
Mollhoff, Iris Natalie
et al.

Publication Date

2020-02-21

DOI

10.1167/iovs.61.2.32

Peer reviewed

Long-term Evolution and Remodeling of Soft Drusen in Rhesus Macaques

Glenn Yiu,[1] Sook Hyun Chung,[1] Iris Natalie Mollhoff,[1] Yinwen Wang,[1] Uyen Tu Nguyen,[1] Bradley Shibata,[1] David Cunefare,[2] Sina Farsiu,[2] Jeffrey Roberts,[3] and Sara M. Thomasy[1,4]

[1]Department of Ophthalmology & Vision Science, University of California, Davis, Sacramento, California, United States
[2]Department of Biomedical Engineering, Duke University, Durham, North Carolina, United States
[3]California National Primate Research Center, Davis, California, United States
[4]Department of Surgical and Radiological Sciences, School of Veterinary Medicine, University of California, Davis, Davis, California, United States

Correspondence: Glenn Yiu, Department of Ophthalmology & Vision Science, University of California, Davis, 4860 Y Street, Suite 2400, Sacramento, CA 95817, USA; gyiu@ucdavis.edu.

Received: August 20, 2019
Accepted: December 5, 2019
Published: February 21, 2020

Citation: Yiu G, Chung SH, Mollhoff IN, et al. Long-term evolution and remodeling of soft drusen in rhesus macaques. *Invest Ophthalmol Vis Sci.* 2020;61(2):32. https://doi.org/10.1167/iovs.61.2.32

Purpose. To characterize the evolution and structure of soft drusen in aged rhesus macaques using in vivo multimodal retinal imaging and ex vivo histologic and ultrastructural analyses as a nonhuman primate model of early age-related macular degeneration (AMD).

Methods. Multimodal imaging including fundus photography, spectral domain optical coherence tomography (SD-OCT), and fundus autofluorescence (FAF) were used to characterize and track individual drusen lesions in 20 aged rhesus macaques (mean age 23.3 ± 2.7 years) with drusenoid lesions over 2 years, followed by semithin histologic analysis and transmission electron microscopy (TEM).

Results. Although most drusen gradually increased in size, a portion spontaneously regressed or collapsed over 2 years. Histologic analyses showed that soft drusen exhibit hypertrophy and dysmorphia of overlying retinal pigment epithelium (RPE), as seen in early and intermediate AMD, but do not exhibit RPE atrophy, RPE migration, or photoreceptor degeneration characteristic of advanced AMD. Ultrastructure of soft drusen showed abundant lipid particles within Bruch's membrane and AMD-related basal linear deposits (BlinD) resembling those in human drusen.

Conclusions. The dynamic remodeling, histologic findings, and ultrastructural features of soft drusen in aged rhesus macaques support nonhuman primates as an animal model of early AMD and reveal important insights into drusen biogenesis and AMD development.

Keywords: drusen, macular degeneration, retina, rhesus macaques, optical coherence tomography

Age-related macular degeneration (AMD) is the leading cause of vision loss in the elderly, and its advanced forms accounts for approximately 20% of legal blindness in North America.[1] Initial stages of AMD are characterized by pigmentary changes and yellow deposits called drusen, which are located between the retinal pigment epithelium (RPE) basal lamina and inner collagenous layer of Bruch's membrane (BM).[2] Later stages may include the development of choroidal neovascularization in neovascular or "wet" AMD and/or geographic atrophy in advanced "dry" AMD.[3] The pathogenesis of AMD is multifactorial, likely resulting from the complex interplay between oxidative stress, lipid accumulation, and immune dysregulation at the neurovascular interface between photoreceptors, RPE, and underlying choriocapillaris vessels.[4] The current mainstay of AMD therapy includes oral antioxidants that reduce the progression of intermediate AMD[5,6] and intraocular injections of antiangiogenesis agents for neovascular AMD,[7] but no treatment exists for atrophic AMD. Hence, a preclinical animal model that possesses the full spectrum of AMD characteristics is imperative for developing effective therapies for this blinding condition.

Early studies reported a high prevalence of drusenoid pathology (30%–74%) in free-ranging rhesus macaques (*Macaca mulatta*) from Cayo Santiago in Puerto Rico,[8–11] whereas other colonies within the continental United States have shown variable prevalences (5%–47%), likely due to differences in environmental conditions, diet, and genetic background.[12–15] Cynomolgus and Japanese macaques (*Macaca fascicularis* and *Macaca fuscata*) also exhibit an early onset form of the disease with a dominant mode of inheritance,[16–21] but the precise genetic basis remains unclear.[20] Rhesus monkeys with drusenoid lesions share genetic polymorphisms in the age-related maculopathy susceptibility 2 (ARMS2) locus with human patients with AMD[22–24] and demonstrate similar protein components within the drusen lesions,[19] suggesting common mechanisms between drusen formation in humans and nonhuman primates.

We recently surveyed geriatric rhesus macaques (age >19 years) at the California National Primate Research Center (CNPRC) and found a 30.7% prevalence of drusenoid lesions.[15] We performed detailed in vivo characterization of these eyes using color fundus photography, blue-peak fundus autofluorescence (FAF), and spectral-domain optical coherence tomography (SD-OCT) and found that only approximately half exhibited imaging features of soft drusen similar to those in human AMD, whereas the remainder resembled the punctate lesions of lipoidal degeneration, a process characterized by engorgement of individual RPE cells with lipid droplets.[25–27] Cynomolgus macaques used in translational studies have also demonstrated similar punctate lesions that are not true soft drusen when evaluated on histology.[28]

Although studies have shown that drusen prevalence in rhesus macaques increases with age,[8,29] these cross-sectional studies are limited by the qualitative nature of fundus images that do not clearly distinguish between drusen phenotypes, absence of longitudinal data to track the evolution of individual lesions, and lack of histologic correlates in the same set of animals. In this study, we employ high-resolution in vivo retinal imaging to track the evolution of individual drusen lesions in aged rhesus monkeys over a period of 2 years, followed by ex vivo histologic and ultrastructural analyses of the same animals. We found that soft drusen in these animals undergo dynamic remodeling, with most showing steady growth and some undergoing regression or collapse. They also exhibit histologic and ultrastructural features of lipid particle accumulation resembling human drusen in early AMD but not the atrophic or neovascular changes associated with progression to advanced AMD. Our detailed characterization of this nonhuman primate model of soft drusen reveals critical insights into the pathogenesis and progression of drusen and AMD.

Methods

Subjects

Animals were sedated with intramuscular injection of ketamine hydrochloride, midazolam, and dexmedetomidine, followed by pupillary dilation with tropicamide (Bausch & Lomb, Tampa, FL, USA) and cycloplegia with cyclopentolate (Akorn, Lake Forest, IL, USA). All animals underwent slit lamp biomicroscopy, dilated fundus biomicroscopy, and rebound tonometry, followed by SD-OCT imaging, FAF, and fundus photography. The CNPRC is accredited by the Association for Assessment and Accreditation of Laboratory Animal Care International. All studies using rhesus macaques (*M. mulatta*) followed the guidelines of the Association for Research in Vision and Ophthalmology Statement for the Use of Animals in Ophthalmic and Vision Research, complied with the National Institutes of Health (NIH) Guide for the Care and Use of Laboratory Animals, and were approved by the University of California, Davis Institutional Animal Care and Use Committee (protocol 20341).

Multimodal Ocular Imaging

SD-OCT and FAF were obtained with SD-OCT using the Spectralis HRA+OCT system (Heidelberg Engineering, Heidelberg, Germany). All animals underwent a 20° × 20° SD-OCT volume scan with 1024 A-scans per B-scan and scan spacing of 25 µm, centered on the fovea, in high-resolution mode, as well as a 30° × 5° SD-OCT raster scan with 1536 A-scans per B-scan and 234-µm spacing between B-scans, in high-resolution enhanced-depth imaging mode. Twenty-five scans were averaged for each B-scan using eye-tracking automatic real-time software (Heidelberg Engineering), and progression mode was enabled using retinal vessel tracking to reliably scan the same area on annual follow-up imaging sessions. Only images with a signal strength of 6 or greater were included for analysis. Confocal scanning laser ophthalmoscopy was used to capture 30° × 30° FAF images using an excitation light of 488 nm and a long-pass barrier filter starting at 500 nm. All in vivo distance and volumetric measurements are nominal and use dimensions of model rhesus macaque eye based on biometric measurements, including corneal curvature and axial length measured from our previous survey of normal animals.[30] Near-infrared imaging was obtained but not analyzed due to the prominent choroidal patterns seen on this modality in rhesus macaques, which limit useful interpretation.[15,31] Fundus photography was performed using the CF-1 Retinal Camera (Canon, Tokyo, Japan) with a 50-degree wide-angle lens. All SD-OCT and FAF imaging was performed by the first author (GY) at CNPRC. Animals were monitored by a trained technician and CNPRC veterinarian at all times.

Image Analysis

SD-OCT images were exported from Heidelberg Explorer software (version 1.8.6.0; Heidelberg Engineering) to the Duke Optical Coherence Tomography Retinal Analysis Program (DOCTRAP, version 62.0),[32,33] a custom image segmentation software designed using MATLAB (MathWorks, Natick, MA, USA) and previously used in OCT image analyses in humans[34,35] and macaques.[30,31] For thickness measurements of the RPE–drusen complex (RPE-DC), segmentation boundaries along the RPE and BM were automatically determined from every horizontal B-scan using DOCTRAP, followed by manual refinement by experienced graders.[36–38] The RPE-DC volume was measured across the central 3-mm and 5-mm circular regions centered on the fovea. Abnormal thickening of the RPE-DC that was more than 2 standard deviations greater than mean age-matched normative data (mean ± SD, 16.5 ± 2.7 µm) as reported[15] was used to generate drusen maps and measure drusen volume as previously described for human subjects enrolled in the Age-Related Eye Diseases Study.[39,40] A change in drusen height greater than 2 standard deviations (5.4 µm) was classified as drusen enlargement or regression, whereas changes less than this threshold were classified as stable. Lesions detected at year 2 but not at baseline were classified as both enlarged and new, whereas those detected at baseline but not at year 2 were classified as both regressed and collapsed.

Histologic Processing

For semithin histologic sections, entire globes (n = 3 per group) were fixed in 2% paraformaldehyde and 0.5% glutaraldehyde for a minimum of 12 hours, with a small slit made through the pars plana with a scalpel blade to facilitate penetration of the fixative. An approximately 15-mm × 5-mm horizontal region of tissue including the optic nerve and central macula was carefully dissected out. Tissues were dehydrated using increasing concentrations

of ethanol from 50% to 100%, preinfiltrated with a 50:50 mixture of ethanol and methylmethacrylate (Technovit; Kulzer, Wehrheim, Germany) for 2 to 3 hours, and then infiltrated with methylmethacrylate for a minimum of 24 hours. Serial sections were cut at a 1.5-μm thickness through the foveal region using a Leica (Wetzlar, Germany) EM UC6 ultramicrotome, with a horizontal orientation along the optic disc- foveal axis matching the SD-OCT line scans. The slides were stained with 1% toluidine blue O in 1% sodium borate for 30 seconds, rinsed, dried, and coverslipped (Permount; Fisher, Hampton, NH, USA). Histologic sections were imaged using a 40× objective lens on a Virtual Slide Microscope (VS120-S6-W; Olympus, Tokyo, Japan) at a resolution of 172.51 nm per pixel. For each eye, we randomly identified 10 soft drusen lesions in the central 3 mm of the macula and measured the height of the druse (from BM to RPE basal lamina), the height of RPE cell at the apex of each druse, and the height of the photoreceptor inner segment (IS) and outer nuclear layer (ONL) overlying the apical RPE using manual calipers on ImageJ (v1.49; NIH, Bethesda, MD, USA).

Electron Microscopy

For transmission electron microscopy (TEM), separate eyes (n = 3 per group) were fixed in 2% paraformaldehyde and 2.5% glutaraldehyde in 0.1 M sodium cacodylate buffer, with fixative injected intravitreally using a 25-gauge needle through the pars plana at the time of necropsy followed by immersion of the entire globe in the fixative to ensure a death-to-preservation time of several seconds. After a minimum of 12 hours of fixation, an approximately 5-mm × 5-mm square region of the macula was dissected, guided by fundus and SD-OCT images to include an area with highest drusen density. The tissues were postfixed with 2% osmium tetroxide, dehydrated with increasing concentrations of ethanol from 50% to 100%, preinfiltrated with propylene oxide and epoxy resin (Poly/Bed 812, Polysciences, Warrngton, PA, USA), and then infiltrated with resin for a minimum of 24 hours. Semithin sections were cut at a 1.5-mm thickness and ultrathin sections were cut at a 100-nm thickness using a Leica EM UC6 ultramicrotome, with a horizontal orientation along the axis of the optic disc and fovea similar to the SD-OCT line-scans. TEM was performed using a Talos L120c system (ThermoFisher Scientific, Hillsboro, OR, USA).

Statistics

Changes in RPE-DC or drusen volume based on in vivo imaging were compared using repeated-measures ANOVA. Comparisons of RPE height, photoreceptor IS and ONL between eyes with soft drusen, punctate lesions, and normal aging based on histologic analyses were assessed by 2-way ANOVA with Bonferroni posttests. Normality was assessed using the Shapiro-Wilks test, where a P value greater than 0.05 was used to reject the null hypothesis. The relationship between drusen height and RPE height was assessed by linear regression analysis. P values less than 0.05 were considered significant for all tests. All statistical analyses were performed using SPSS Statistics (version 22; IBM, Armonk, NY, USA).

Results

Multimodal In Vivo Imaging of Soft Drusen

We previously identified 20 animals (mean age 23.3 ± 2.7 years) that exhibited drusenoid lesions by dilated fundus biomicroscopy from a cohort of 65 aged macaques evaluated at CNPRC.[15] Among eyes with drusenoid lesions and fundus images of adequate quality, 47% demonstrated soft drusen, which appear as yellow-white lesions with indistinct borders (Fig. 1A), whereas the remaining eyes exhibit fine, punctate lesions, which are smaller and more uniform in size (Fig. 1B), as previously described.[15] Both soft drusen and punctate lesions are variably hyperautofluorescent on blue-peak FAF (Figs. 1D, 1E). SD-OCT revealed that only soft drusen exhibit dome-shaped elevation of the RPE over BM, with upward deflection of overlying outer retinal bands corresponding to the external limiting membrane, ellipsoid zone, and interdigitation zone (Figs. 1G, 1J). By contrast, eyes with the punctate lesions (Figs. 1H, 1K) or normal aging (Figs. 1I, 1L) showed no visible abnormalities on SD-OCT. We detected no cases of calcified drusen or subretinal drusenoid deposits (SDDs) or evidence of pigmentary changes on fundus photography, which in humans portends a higher risk for progression to advanced forms of AMD.[41]

Two-Year Change in Drusen Volume

We monitored the evolution of soft drusen in these rhesus macaques over 2 years using FAF (Figs. 2A, 2B) and SD-OCT (Figs. 2C, 2F) with retinal vessel tracking for image registration. Semiautomated segmentation of the RPE-DC from these images provided detailed three-dimensional thickness maps of the RPE-DC in the 5-mm diameter circular region centered on the fovea (Figs. 2G, 2H).[39,42,43] Eyes with soft drusen exhibited a gradual increase in RPE-DC volume over time (P = 0.015), with a mean increase of 0.018 mm^3 (4.6%) at year 1 and 0.035 mm^3 (9.2%) at year 2, whereas eyes with punctate lesions (P = 0.189) or no drusenoid lesions (P = 0.173) did not change with time (Fig. 2I). Abnormal thickening of the RPE-DC that was more than 2 standard deviations greater than mean age-matched normative data[15] was used to generate drusen maps (Figs. 2J, 2K) and measure drusen volume as previously described in human studies.[39] Soft drusen volume increased significantly over the 2 years (P = 0.009), with a mean increase of 0.012 mm^3 (42%) at year 1 and 0.025 mm^3 (86%) at year 2, whereas eyes with punctate lesions again showed no significant change with time (P = 0.158; Fig. 2L). These values are comparable to drusen volume changes in human eyes with AMD without signs of geographic atrophy.[39,44] Thus, consistent with cross-sectional studies showing increased drusen prevalence with age, our longitudinal study in macaques shows that soft drusen burden increases at a quantifiable rate over time, similar to those in human AMD.

Dynamic Remodeling of Soft Drusen

Although most drusen increased in size, we noted that a small number of lesions regressed or completely collapsed (Figs. 2E, 2F, 2J, 2K), with no subsidence of the outer plexiform or inner nuclear layers, disruption of outer retinal layers, or signal hypertransmission below BM that often precedes the development of geographic atrophy in human AMD.[45,46] We also did not detect any evidence of

Investigative Ophthalmology & Visual Science

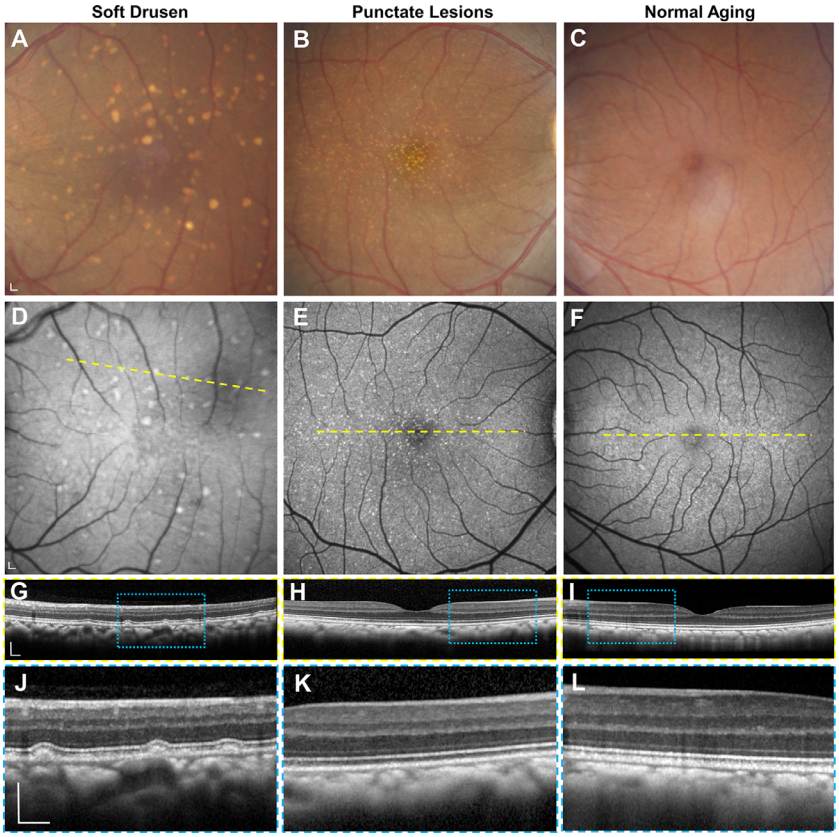

Figure 1. Multimodal imaging of rhesus macaque eyes with drusenoid lesions. Representative images of (**A–C**) color fundus photography, (**D–F**) fundus autofluorescence, and (**G–L**) SD-OCT of the macular region of macaque eyes with (**A**, **D**, **G**, **J**) soft drusen, (**B**, **E**, **H**, **K**) punctate lesions, and (**C**, **F**, **I**, **L**) normal aging. SD-OCT scans in **G–I** correspond to the location of the *yellow dashed lines* in **D–F**. Magnified views in **J–L** correspond to the *blue-dashed regions* in **G–I**. *Scale bars*: 200 μm.

intraretinal or subretinal fluid or other characteristics of choroidal neovascularization as seen in neovascular AMD. The soft drusen uniformly exhibited homogeneous internal reflectivity (Fig. 3A), in contrast to soft drusen in human patients with AMD, which may exhibit variably reflective drusen substructures and intraretinal hyperreflective foci (Fig. 3B) that predict progression to advanced, atrophic AMD.[47–49]

Using registered SD-OCT volumes, we labeled the positions of individual drusen lesions at years 0 and 2 (Figs. 4A–4D) and measured the change in RPE-DC and drusen height over the 2 years (Figs. 4E, 4F). Change in drusen height greater than 2 standard deviations of mean age-matched normative data[15] was considered to have significantly increased or regressed in size. We found that although most lesions remained stable (27.9%) or grew (25.9%) over the 2 years, a portion regressed in size (9.8%; Figs. 4F, 4G). We found that 25.6% of lesions appeared de novo at year 2 and 10.7% appeared to have completely collapsed after 2 years. These results suggest that although drusen burden increases with time, some lesions undergo regression or collapse consistent with drusen remodeling seen on SD-OCT in humans[48,50,51] but exhibit none of the imaging features predicting progression to geographic atrophy in advanced AMD in humans.

To better understand the relationship between drusen growth and retinal location, we also compared the change in height of drusen in the central 1-mm region, 3-mm inner ring, and 5-mm outer ring (Supplementary Fig. S1). Most of the drusen were located in the 3-mm inner ring, and few were located in the central 1-mm foveal region (Supplementary Figs. S1A–S1C). Interestingly, the drusen at the fovea were more likely to remain stable, whereas those in the 5-mm outer ring were more likely to be new (Supplementary Figs. S1D–S1F). Although the variability between animals limits our interpretation of this difference, future studies on the relationship between drusen location and growth warrant further investigation.

Semithin Histology of Soft Drusen

Methacrylate-embedded semithin (1.5-μm) histologic sections provide excellent preservation of chorioretinal anatomy and reliable measurements of chorioretinal layers when compared with in vivo SD-OCT in rhesus macaques.[30] We analyzed semithin histologic sections from six eyes of six animals (three with soft drusen, one with punctate lesions, and two age-matched normals) that underwent necropsy after the 2-year period to evaluate the ex vivo anatomic correlate to the in vivo morphology seen on live imaging. Consistent with the appearance on SD-OCT (Figs. 5A–5C), soft drusen appear as dome-shaped deposits between the basal lamina of the RPE and BM and consist of amorphous material and round droplets representing

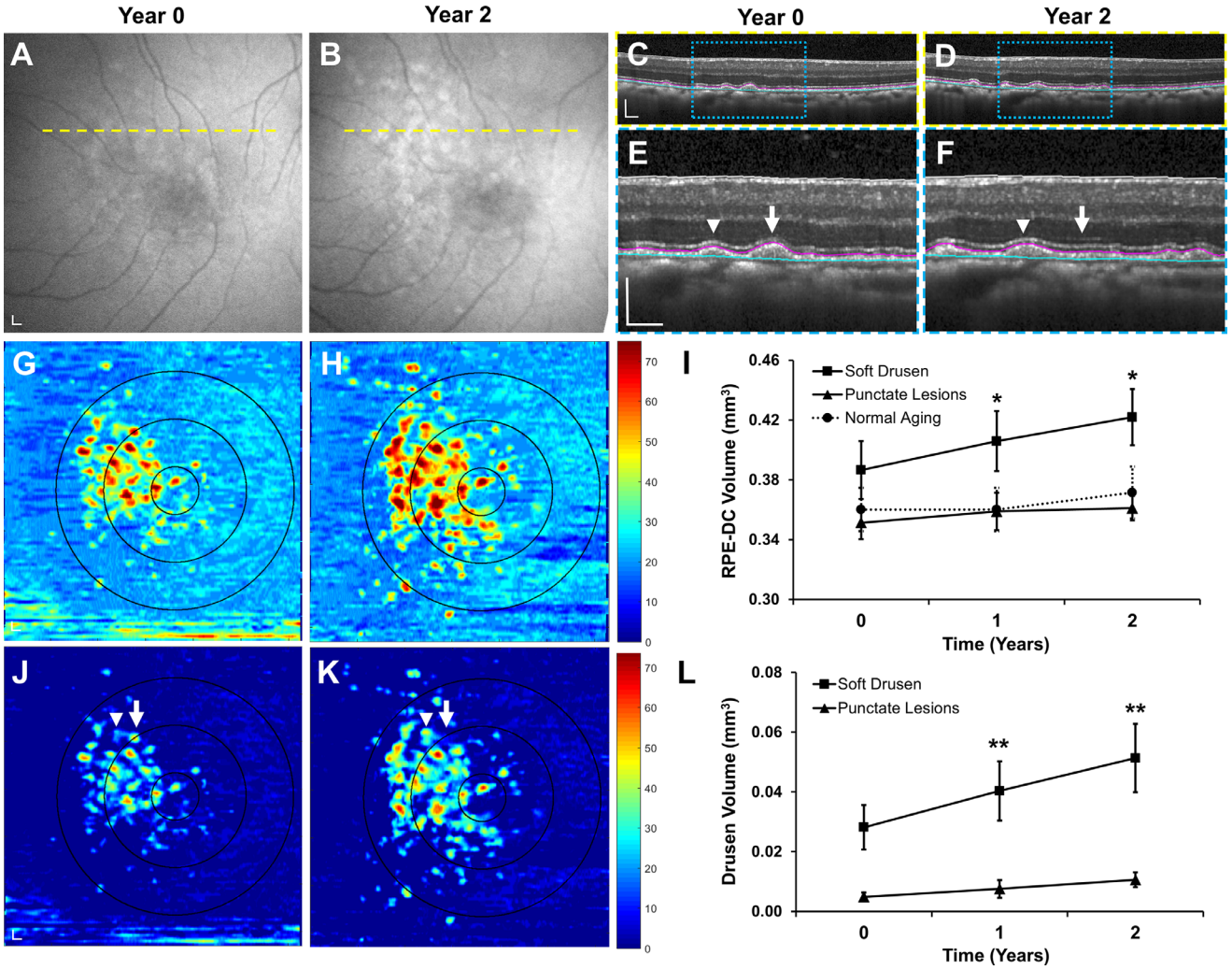

Figure 2. Progression of soft drusen volume in rhesus macaques over 2 years. Representative images of (**A**, **B**) fundus autofluorescence and (**C**, **F**) SD-OCT of an eye with soft drusen at years 0 and 2. SD-OCT scans in **C** and **D** correspond to the *yellow dashed lines* in **A** and **B**. Magnified views in **E** and **F** correspond to *blue-dashed regions* in **C** and **D**. Although most soft drusen increased in size (*arrowheads*) over 2 years, some lesions regressed or collapsed (*arrow*). Segmentation of the RPE (*magenta line*) and Bruch's membrane (*cyan line*) in **C–F** were used to generate (**G**, **H**) RPE-DC maps and measure (**I**) change in RPE-DC volume in the 5-mm-diameter circular region from years 0 to 2. The concentric circles in **G** and **H** represent the corresponding 1-mm-, 3-mm-, and 5-mm-diameter regions centered on the fovea at different time points. Abnormal thickening of the RPE-DC more than 2 standard deviations greater than mean age-matched normative data was used to generate (**J**, **K**) drusen maps and measure (**L**) change in drusen volume within the central 5-mm-diameter region. Data are presented as means ± SEM. $N = 5$ animals (10 eyes) per group. *$P < 0.05$. **$P < 0.01$. *Scale bars*: 200 μm.

lipid pools (Figs. 5D–5G), as described by the Sarks et al.,[52–55] and likely represent partially preserved lipoproteins as reported by Curcio and colleagues.[56–61] The soft drusen are sometimes contiguous with basal linear deposits (BlinD; Fig. 5E), although we did not observe significant basal laminar deposits (BlamD)—thickening of the RPE basement membrane commonly seen in both AMD and normal human aging.[52,54,62] We also did not detect evidence of SDDs or refractile spherules inside drusen representing hydroxyapatite[63,64] seen in some human patients with AMD, although we cannot exclude the possibility that differences in tissue preservation, fixation, or sampling strategy (e.g., if tissues were sampled with stepped or serial sections) may limit our ability to detect these lesions.

The RPE cells overlying soft drusen appear hypertrophic and dysmorphic, with randomly distributed spindle-shaped melanosomes compared with normal RPE cells where melanosomes are typically located apically (Figs. 5E, 5G). The mean height of RPE cells overlying soft drusen was significantly higher than RPE adjacent to the lesions (14.7 ± 4.7 μm vs. 11.1 ± 1.5 μm; $P < 0.001$) or RPE in the macula of eyes with punctate lesions or normal aging (Fig. 5H). We did not detect significant RPE atrophy or any intraretinal migration of RPE cells, which are histologic correlates of hyperreflective foci seen on SD-OCT (Fig. 3B)[62,65] and precursors to geographic atrophy in human AMD.[47] Interestingly, there was also a slight but significant association between the height of soft drusen and height of overlying RPE cells ($R^2 = 0.280$, $P = 0.003$; Fig. 5I), suggesting that larger drusen lesions may be associated with a greater degree of RPE hypertrophy.

Although photoreceptor outer segments are variably preserved on semithin histology, both the IS and ONL overlying the soft drusen appeared grossly normal compared

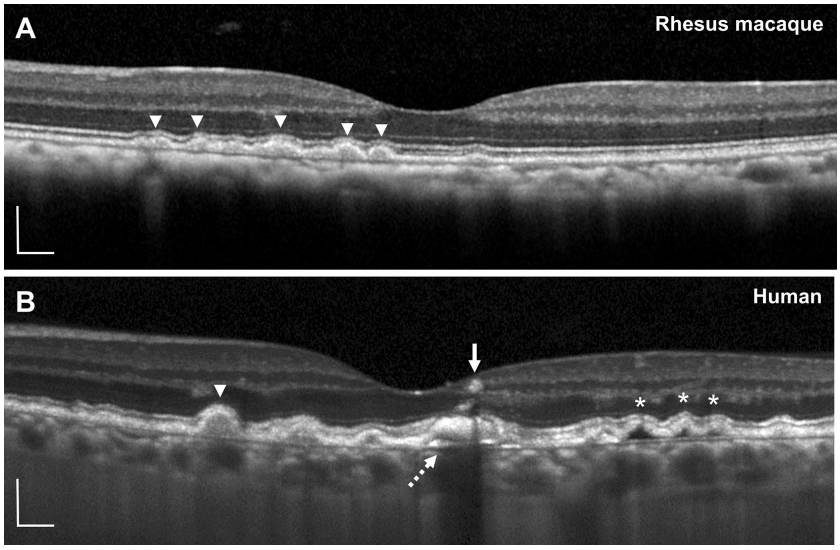

Figure 3. Comparison of soft drusen in rhesus macaques and humans using SD-OCT. Representative SD-OCT images of soft drusen in (**A**) rhesus macaques and (**B**) a 74-year-old human participant with intermediate nonneovascular AMD. Soft drusen in rhesus macaques uniformly exhibit homogeneous internal reflectivity similar to some in human AMD (*arrowheads*). Human drusen may have complex drusen substructures (*dashed arrow*), hyporeflective cores (*asterisks*), and intraretinal hyperreflective foci (*arrow*). *Scale bars*: 200 μm.

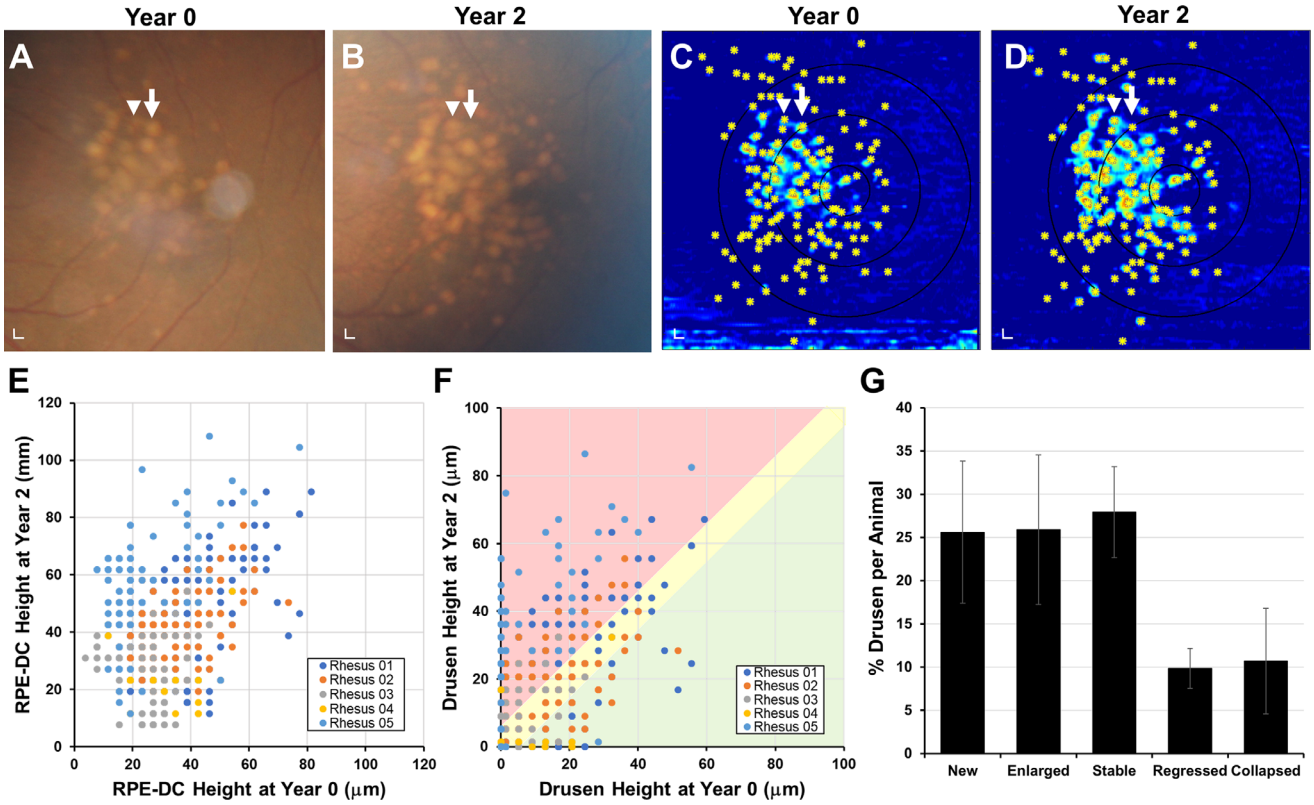

Figure 4. Evolution of individual drusen lesions in rhesus macaques over 2 years. Representative images of (**A**, **B**) color fundus photographs from the eye shown in Figure 2 at years 0 and 2, showing growth of some drusen (*arrowhead*) and collapse of others (*arrow*). (**C**, **D**) Corresponding drusen maps with each druse manually labeled (*asterisks*) allowed measurement of the change in (**E**) RPE-DC height and (**F**) drusen height at each location for five rhesus macaques at years 0 and 2. Over the 2 years, many drusen were new (on *vertical axis*) or increased in size (*red-shaded area*), although some remained stable (*yellow-shaded area*), and a minority regressed (*green-shaded area*) or completely collapsed (on *horizontal axis*). (**G**) Bar graph comparing the proportion of new, enlarged, stable, regressed, and collapsed drusen in this cohort of animals. Data are presented as means ± SEM. $N = 5$ animals (10 eyes) per group. *Scale bars*: 200 μm.

Investigative Ophthalmology & Visual Science

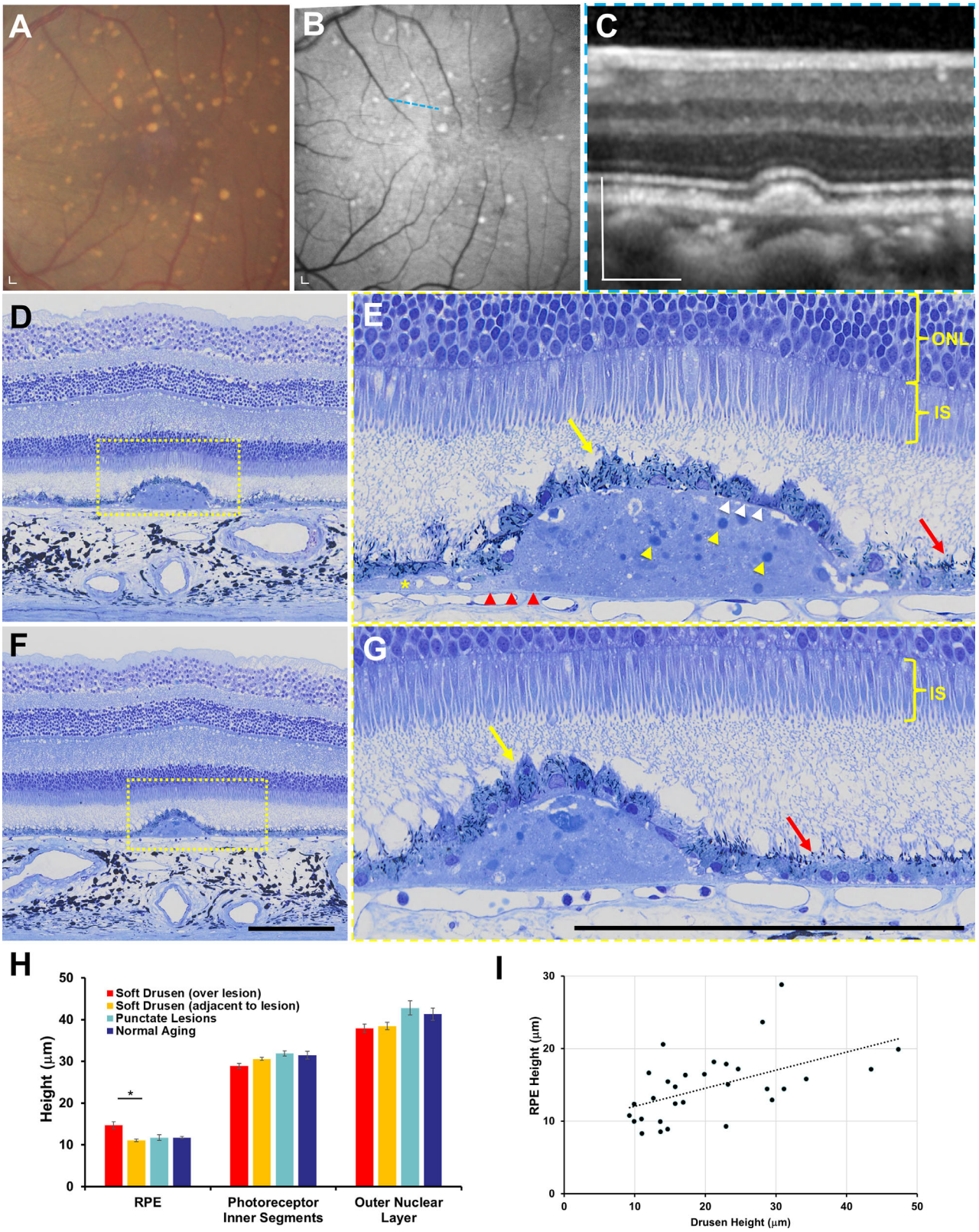

Figure 5. Semithin histologic analysis of soft drusen in rhesus macaques. (**A**) Color fundus photograph and (**B**) fundus autofluorescence image of the macular region of an eye with soft drusen, along with (**C**) SD-OCT image scan along the *blue dashed line* in **B**. (**D**, **E**) Semithin histologic section across the same druse seen in **C** shows soft drusen to be dome-shaped deposits between the basal lamina of the RPE (*white arrowheads*) and BM (*red arrowheads*) consisting of amorphous material and round droplets representing lipid pools (*yellow arrowheads*), which extend beyond the border of the mound as basal linear deposits (BlinD, *yellow asterisk*). The RPE cells overlying drusen (*yellow arrow*) are hypertrophic and dysmorphic with scattered melanosomes, although more normal-appearing RPE cells adjacent to the drusen

Investigative Ophthalmology & Visual Science

(*red arrow*) have melanosomes that are located along the apical processes. The photoreceptor inner segments (IS) and outer nuclear layer (ONL) overlying drusen appear normal compared to adjacent regions. (**F**, **G**) Semithin histologic sections of a different soft druse showing again the hypertrophic and dysmorphic RPE overlying the lesion (*yellow arrow*) and more normal-appearing RPE with apically located melanosomes (*red arrow*) nearby. Photoreceptor outer segments were not well preserved in these sections. The magnified views in **E** and **G** correspond to the *yellow-dashed regions* in **D** and **F**. *Scale bars*: 200 μm. (**H**) Bar graphs comparing height of RPE cells, photoreceptor IS, and ONL in regions overlying and adjacent to lesions in eyes with soft drusen (*orange bars*) and in eyes with punctate lesions (*blue bars*) and no lesions/normal aging (*green bars*). Data are presented as means ± SEM. $N = 3$ animals (3 eyes) per group. $^*P < 0.05$.

with adjacent areas without drusen and did not exhibit the photoreceptor degeneration typically seen in more advanced forms of AMD. The photoreceptor IS overlying drusen was slightly shorter than those in adjacent areas (28.9 ± 3.5 μm vs. 30.6 ± 1.9 μm; $P = 0.009$), but the mean heights of the ONL were similar (37.9 ± 5.3 μm vs. 38.4 ± 4.9 μm; $P = 0.510$; Fig. 5H). We also noted no choriocapillary loss or degeneration beneath soft drusen, although we cannot exclude the possibility of preserved "ghost" vessels without immunostaining for endothelial cells.[66] Together, our data suggest that although soft drusen in rhesus monkeys exhibit many features of soft drusen in human AMD, they lack features such as thick BlamD, RPE atrophy, intraretinal RPE migration, or photoreceptor degeneration found in advanced disease.

Ultrastructure of Soft Drusen

We performed TEM on eyes from two animals with soft drusen, two animals with punctate lesions, and three aged controls to assess the ultrastructural correlates to the in vivo ocular imaging features. Similar to initial descriptions in human drusen by the Sarks et al.[52] and further elaboration by Curcio and colleagues,[56–61] we found that soft drusen appear as dome-shaped mounds between RPE basal lamina and internal collagenous layer of BM. Their interiors consist of "membranous debris" and vesicular particles, which are heterogeneous in size and appearance, with an electron-dense exterior and a more lucent interior likely representing lipoprotein particles that were partially extracted by tissue processing (Figs. 6A–6F). The particles extend beyond the borders of the drusen mounds to form a discrete sublayer external to the RPE basal lamina analogous to BlinD in human AMD (Figs. 6D, 6G, 6H). These findings support the notion that drusen and BlinD are focal and diffuse forms of the same lipoprotein accumulation in both humans and macaques. These particles are also present within BM, analogous to the age-related lipid accumulation in human BM and sometimes referred to as pre-BlinD.[57,67,68] Similar to human aging,[69] there were scant RPE basal infoldings in these aged macaque eyes (Fig. 6B). Interestingly, we did not find significant electron-dense material internal to the RPE basal lamina resembling BlamD in human AMD (Fig. 6F)[52,54,62] or evidence of SDDs in macaques. Hence, although rhesus monkeys exhibit the ultrastructural features of soft drusen and BlinD characteristic of human early AMD, they do not show features such as BlamD or SDDs that may be associated with more advanced AMD.

Eyes with punctate lesions exhibited individual RPE cells with lipid-filled vacuoles of different electron densities likely due to variable lipid extraction (Figs. 7A, 7B) and are consistent with lipoidal degeneration as previously reported in macaques.[25–27] The lipid-filled cells appear to have normal melanosomes but fewer lipofuscin granules (Figs. 7A, 7B). These eyes also demonstrate lipid particles in sublayers external to RPE basal lamina as BlinD and within BM as pre-BlinD (Figs. 7C–7F), with some showing disruption of the RPE basal lamina and lipid particles extending into the RPE cytoplasm (Figs. 7E, 7F). In comparison, normal aged macaque eyes without visible lesions showed no drusen or BlinD (Figs. 7G, 7H), more prominent RPE basal infoldings (Fig. 7H), and scant lipid particles within BM (Fig. 7H). These data suggest that aged eyes with punctate lesions have lipoidal degeneration and also ultrastructural features of lipid accumulation seen in eyes with soft drusen.

Discussion

Development of treatments for AMD has been hindered by the lack of good animal models that exhibit the full spectrum of nonneovascular AMD features ranging from early drusen to advanced geographic atrophy. Antiangiogenesis agents that had revolutionized the management of neovascular AMD were successfully developed using a laser-induced model of choroidal neovascularization that could be generated in various animal species.[70] However, the degenerative features of AMD are difficult to simulate because laboratory rodents have a short life span and do not possess a macula. Hence, although mouse models reveal insights into the role of oxidative stress, lipid accumulation, and inflammation in aging and AMD,[58] none exhibit the features seen in human soft drusen in AMD.

Nonhuman primates are the only mammalian species beside humans to possess a true macula and can also serve as a model of inherited cone-based retinal degeneration.[71] Here, we present the first study to combine long-term, longitudinal imaging of soft drusen in macaques with detailed structural characterization of these same lesions ex vivo. The use of high-resolution SD-OCT with retinal vessel tracking allowed us to track the fate of individual lesions, and scheduled necropsies of these animals enabled near-instantaneous death-to-preservation time to provide unprecedented, high-quality histology and ultrastructure. We found that soft drusen in macaques undergo dynamic remodeling and exhibit the lipid particle accumulation seen in human drusen in early AMD but lack the RPE degeneration associated with advanced atrophic AMD.

The mechanism for drusen biogenesis in humans has been deduced from their composition on ultrastructure, which includes round vesicular bodies initially termed *membranous debris*,[53–55] which on lipid-preserving postfixation appear to be lipoprotein particles secreted basolaterally by the RPE into BM.[58,60,61] In our study, TEM of soft drusen in macaques also demonstrated similar lipid particles within focal and diffuse deposits in the RPE sublamina and within BM closely resembling soft drusen, BlinD, and pre-BlinD in human AMD. The presence of BlinD and pre-BlinD in eyes with lipoidal degeneration suggests that earlier forms of the same lipid accumulation process may occur even in macaques without a funduscopic appearance of soft drusen and may explain the BM thickening seen on OCT in these

Investigative Ophthalmology & Visual Science

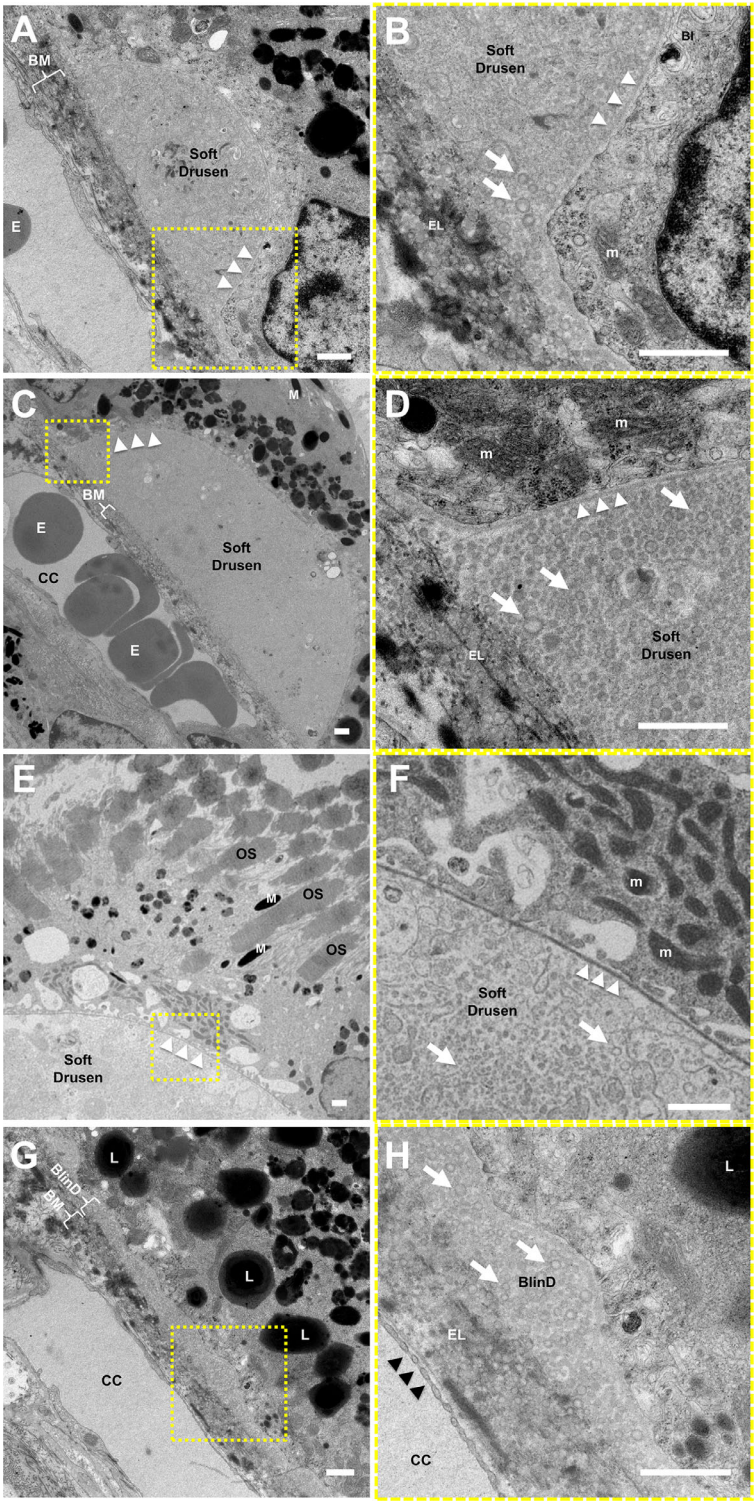

Figure 6. Ultrastructure of soft drusen in rhesus macaques. TEM images of (**A**, **B**) a small soft druse, (**C–F**) larger drusen, and (**G**, **H**) thin basal linear deposits (BlinD) located between the RPE basal lamina (*white arrowheads*) and Bruch's membrane (BM). The magnified views in **B**, **D**, **F**, and **H** correspond to the *dashed-yellow areas* in **A**, **C**, **E**, and **G**. The neurosensory retina is located at the *upper right* and the choroid/sclera are toward the *lower left*. The soft drusen in **A–F** and BlinD in **G** and **H** are both largely composed of vesicular particles with an electron-dense exterior and electron-lucent interior (*arrows*) consistent with partially extracted lipoprotein particles. Melanosomes (M), lipofuscin granules (L), and mitochondria (m) in RPE cells; overlying photoreceptor outer segments (OS); and erythrocytes (E) in the choriocapillaris (CC) can also be seen. The elastic layer (EL) of BM, scant RPE basal infoldings (BI), and fenestrations of the CC (*black arrowheads*) are better seen on the magnified views. *Scale bars*: 1 μm.

Investigative Ophthalmology & Visual Science

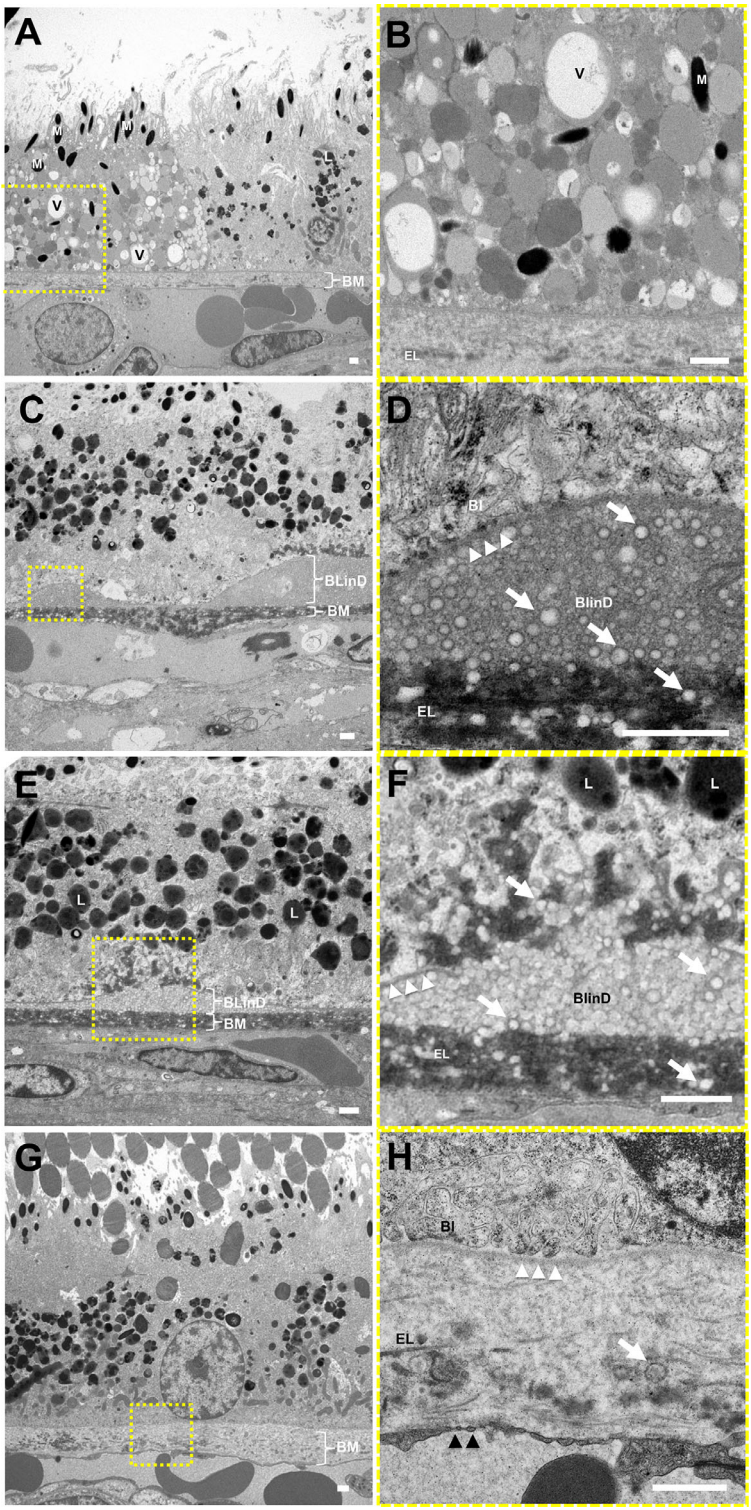

Figure 7. Ultrastructure of RPE lipoidal degeneration and extracellular lipid accumulation in rhesus macaques. TEM of eyes with punctate lesions without soft drusen show (**A**, **B**) individual RPE cells that appear swollen with vacuoles (V) and granules of various electron densities, likely lipid-filled, grossly normal melanosomes (M), and few lipofuscin granules (L), consistent with lipoidal degeneration. These eyes also exhibit (**C**, **D**) basal linear deposits (BlinD) of lipid particles (*white arrows*) located between the RPE basal lamina (*white arrowheads*) and Bruch's membrane (BM), and (**E**, **F**) areas showing the lipid particles extending beyond the RPE basal lamina into the RPE cytoplasm and into BM itself. By contrast, (**G**, **H**) normal aged eyes without visible lesions show no drusen or BlinD, rare lipid particles in BM (*white arrow*), and normal-appearing RPE cells with basal infoldings (BI). The magnified views in **B**, **D**, **F**, and **H** correspond to the *dashed-yellow areas* in **A**, **C**, **E**, and **G**. The neurosensory retina is located at the *top* and the choroid/sclera are toward the *bottom*. The elastic layer (EL) of BM, scant RPE basal infoldings (BI), and fenestrations of the CC (*black arrowheads*) are better seen on the magnified views. *Scale bars*: 1 μm.

Investigative Ophthalmology & Visual Science

eyes.[15] High-performance liquid chromatography of BM extracts from human AMD has found these lipoproteins to be cholesterol rich and, importantly, fatty acids dominated by linoleate rather than docosahexaenoate, which implicates a dietary source rather than phagocytized photoreceptor outer segments.[72,73] This may have important implications for this nonhuman primate model of drusen, where dietary modifications may potentially impact the progression of maculopathy.[74] Recent studies using oral simvastatin in patients with AMD demonstrated evidence of drusen regression[75,76]—a hypothesis that could be tested in rhesus macaques in a more controlled manner.

Beyond the similarities between macaque and human drusen, the unique differences between the two species are also interesting. SD-OCT of soft drusen in macaques demonstrates homogeneous internal reflectivity. By contrast, SD-OCT of human AMD exhibits heterogenous internal reflectivity of drusen representing calcified nodules[77] and intraretinal hyperreflective foci representing RPE migration[62,65]—features that portend progression to atrophic AMD. Histologic correlates in rhesus monkeys also revealed hypertrophic and dysmorphic RPE but no RPE atrophy, RPE migration, photoreceptor degeneration, or SDDs typically seen preceding geographic atrophy. We hypothesize that drusen development and remodeling in macaques may occur without RPE loss or geographic atrophy and that soft drusen may be required but not sufficient to trigger advanced, atrophic AMD. The absence of SDDs, which accumulate apical to RPE,[78] may suggest differences in lipid transport across the apical surfaces of polarized RPE cells in different primate species, although the preponderance of soft drusen and BlinD over BlamD in macaques may reveal mechanistic insight into lipid retention across the RPE basal lamina that enables these animals to clear BlamD more effectively than humans and avoid atrophy. The punctate lesions of lipoidal degeneration are another feature uniquely seen at high frequencies in aged nonhuman primates as previously shown.[15,25–27] We did not find evidence of these lesions as a precursor to soft drusen during the 2-year follow-up of our cohort. Instead, lipoidal degeneration may be yet another manifestation of lipid accumulation in macaques that is distinct from the processes that promote AMD progression in humans. Finally, differences in uveal pigmentation between macaques and humans may contribute to differences in oxidative stress in addition to lipid metabolism.[31]

Together, our data suggest that rhesus macaques may serve as an important model for macular lipid accumulation and drusen biogenesis, rather than as a model for AMD progression and geographic atrophy, which is critical for evaluating clinical biomarkers and therapies for earlier stages of AMD. Limitations of our study include the small number of animals and limited duration of follow-up of 2 years. However, although the development of more advanced phenotypes may require longer follow-up, many of the animals in this study died due to natural circumstances after the 2-year follow-up, suggesting that we are observing anatomic findings at the very end of the animals' life span and that more late-stage findings typically seen in advanced AMD may be absent in rhesus macaques. Our study showed, for the first time, dynamic remodeling of soft drusen in rhesus macaques, with accumulation and some regression of individual lesions over time but no evidence of progression to geographic atrophy, challenging the assumption in humans that drusen remodeling may be integral to atrophy and disease progression.[44,79,80] Although this may reflect the environment and diet of primates in captivity, the use of primate species possessing maculae provides the unique opportunity to study drusen evolution under controlled conditions, with the potential to further investigate the role of lipid accumulation,[58] immune pathways,[81] or hemodynamic contributions[82,83] to AMD pathogenesis. The aged rhesus macaques used in this study represent only a portion of the CNPRC aged rhesus resource, which includes over 100 animals older than 19 years and 100 recruitment animals in the 15- to 18-year age range. Future efforts to manipulate dietary fat intake or modulate oxidative stress could help trigger more advanced atrophic AMD in these animals, providing a comprehensive model with the full spectrum of AMD characteristics for translational research.

Acknowledgments

Supported by the California National Primate Research Center pilot grant program and base grant NIH P510D011107. A portion of the aged rhesus studied is supported by the NIA Set Aside program. Supported by NIH K08 EY026101, NIH R21 EY031108, the E. Matilda Ziegler Foundation for the Blind, Barr Foundation for Retinal Research, ARVO Foundation, and Macula Society (GY). Supported by NIH P30 EY005722 (SF). Supported by NIH K08 EY021142 and U24 U24EY029904 (ST). Histologic and ultrastructural studies were conducted at the Center for Vision Sciences structure-function core facility, which is supported by NIH P30 EY012576. No funding organizations had any role in the design or conduct of this research. The content is solely the responsibility of the authors and does not necessarily represent the official views of the funding agencies.

Disclosure: **G. Yiu,** Alimera (C), Allergan (C), Carl Zeiss Meditec (C), Clearside Biomedical (F), Genentech (F,C), Iridex (F,C), Verily (C); **S.H. Chung,** None; **I.N. Mollhoff,** None; **Y. Wang,** None; **U.T. Nguyen,** None; **B. Shibata,** None; **D. Cunefare,** None; **S. Farsiu,** None; **J. Roberts,** None; **S.M. Thomasy,** None

References

1. Holz FG, Strauss EC, Schmitz-Valckenberg S, van Lookeren Campagne M. Geographic atrophy: clinical features and potential therapeutic approaches. *Ophthalmology*. 2014;121:1079–1091.
2. Li M, Huisingh C, Messinger J, et al. histology of geographic atrophy secondary to age-related macular degeneration: a multilayer approach. *Retina*. 2018;38:1937–1953.
3. Age-Related Eye Disease Study Research Group. The Age-Related Eye Disease Study system for classifying age-related macular degeneration from stereoscopic color fundus photographs: the Age-Related Eye Disease Study Report Number 6. *Am J Ophthalmol*. 2001;132:668–681.
4. Bowes Rickman C, Farsiu S, Toth CA, Klingeborn M. Dry age-related macular degeneration: mechanisms, therapeutic targets, and imaging. *Invest Ophthalmol Vis Sci*. 2013;54:ORSF68–ORSF80.
5. Age-Related Eye Disease Study Research Group. A randomized, placebo-controlled, clinical trial of high-dose supplementation with vitamins C and E, beta carotene, and zinc for age-related macular degeneration and vision loss: AREDS report no. 8. *Arch Ophthalmol*. 2001;119:1417–1436.
6. Age-Related Eye Disease Study 2 Research Group. Lutein + zeaxanthin and omega-3 fatty acids for age-related macular degeneration: the Age-Related Eye Disease Study 2 (AREDS2) randomized clinical trial. *JAMA*. 2013;309:2005–2015.

7. Todorich B, Yiu G, Hahn P. Current and investigational pharmacotherapeutic approaches for modulating retinal angiogenesis. *Expert Rev Clin Pharmacol*. 2014;7:375–391.
8. Hope GM, Dawson WW, Engel HM, Ulshafer RJ, Kessler MJ, Sherwood MB. A primate model for age related macular drusen. *Br J Ophthalmol*. 1992;76:11–16.
9. El-Mofty A, Gouras P, Eisner G, Balazs EA. Macular degeneration in rhesus monkey (*Macaca mulatta*). *Exp Eye Res*. 1978;27:499–502.
10. Dawson WW, Ulshafer RJ, Engel HM, Hope GM, Kessler MJ. Macular disease in related rhesus monkeys. *Doc Ophthalmol*. 1989;71:253–263.
11. Engel HM, Dawson WW, Ulshafer RJ, Hines MW, Kessler MJ. Degenerative changes in maculas of rhesus monkeys. *Ophthalmologica*. 1988;196:143–150.
12. Monaco WA, Wormington CM. The rhesus monkey as an animal model for age-related maculopathy. *Optom Vis Sci*. 1990;67:532–537.
13. Stafford TJ, Anness SH, Fine BS. Spontaneous degenerative maculopathy in the monkey. *Ophthalmology*. 1984;91:513–521.
14. Olin KL, Morse LS, Murphy C, et al. Trace element status and free radical defense in elderly rhesus macaques (*Macaca mulatta*) with macular drusen. *Proc Soc Exp Biol Med*. 1995;208:370–377.
15. Yiu G, Tieu E, Munevar C, et al. In vivo multimodal imaging of drusenoid lesions in rhesus macaques. *Sci Rep*. 2017;7:15013.
16. Nishiguchi KM, Yokoyama Y, Fujii Y, et al. Analysis of macular drusen and blood test results in 945 *Macaca fascicularis*. *PLoS One*. 2016;11:e0164899.
17. Nicolas MG, Fujiki K, Murayama K, et al. Studies on the mechanism of early onset macular degeneration in cynomolgus (*Macaca fascicularis*) monkeys. I. Abnormal concentrations of two proteins in the retina. *Exp Eye Res*. 1996;62:211–219.
18. Suzuki MT, Terao K, Yoshikawa Y. Familial early onset macular degeneration in cynomolgus monkeys (*Macaca fascicularis*). *Primates*. 2003;44:291–294.
19. Umeda S, Suzuki MT, Okamoto H, et al. Molecular composition of drusen and possible involvement of anti-retinal autoimmunity in two different forms of macular degeneration in cynomolgus monkey (*Macaca fascicularis*). *FASEB J*. 2005;19:1683–1685.
20. Umeda S, Ayyagari R, Allikmets R, et al. Early-onset macular degeneration with drusen in a cynomolgus monkey (*Macaca fascicularis*) pedigree: exclusion of 13 candidate genes and loci. *Invest Ophthalmol Vis Sci*. 2005;46:683–691.
21. Pennesi ME, Garg AK, Feng S, et al. Measuring cone density in a Japanese macaque (*Macaca fuscata*) model of age-related macular degeneration with commercially available adaptive optics. *Adv Exp Med Biol*. 2014;801:309–316.
22. Francis PJ, Appukuttan B, Simmons E, et al. Rhesus monkeys and humans share common susceptibility genes for age-related macular disease. *Hum Mol Genet*. 2008;17:2673–2680.
23. Singh KK, Krawczak M, Dawson WW, Schmidtke J. Association of HTRA1 and ARMS2 gene variation with drusen formation in rhesus macaques. *Exp Eye Res*. 2009;88:479–482.
24. Pahl L, Spangenberg A, Schubert S, Schonmann U, Schmidtke J, Stuhrmann M. Characterization of the 10q26-orthologue in rhesus monkeys corroborates a functional connection between ARMS2 and HTRA1. *Exp Eye Res*. 2012;98:75–78.
25. Fine BS, Kwapien RP. Pigment epithelial windows and drusen: an animal model. *Invest Ophthalmol Vis Sci*. 1978;17:1059–1068.
26. Feeney-Burns L, Malinow R, Klein ML, Neuringer M. Maculopathy in cynomolgus monkeys: a correlated fluorescein angiographic and ultrastructural study. *Arch Ophthalmol*. 1981;99:664–672.
27. Anderson M, Dawson WW, Gonzalez-Martinez J, Curcio CA. Drusen and lipid-filled retinal pigment epithelium cells in a rhesus macula. *Vet Ophthalmol*. 2006;9:201–207.
28. Rudolf M, Curcio CA, Schlotzer-Schrehardt U, et al. Apolipoprotein A-I mimetic peptide L-4F removes Bruch's membrane lipids in aged nonhuman primates. *Invest Ophthalmol Vis Sci*. 2019;60:461–472.
29. Gouras P, Ivert L, Landauer N, Mattison JA, Ingram DK, Neuringer M. Drusenoid maculopathy in rhesus monkeys (*Macaca mulatta*): effects of age and gender. *Graefes Arch Clin Exp Ophthalmol*. 2008;246:1395–1402.
30. Yiu G, Wang Z, Munevar C, et al. Comparison of chorioretinal layers in rhesus macaques using spectral-domain optical coherence tomography and high-resolution histological sections. *Exp Eye Res*. 2018;168:69–76.
31. Yiu G, Vuong VS, Oltjen S, et al. Effect of uveal melanocytes on choroidal morphology in rhesus macaques and humans on enhanced-depth imaging optical coherence tomography. *Invest Ophthalmol Vis Sci*. 2016;57:5764–5771.
32. Chiu SJ, Toth CA, Rickman BC, Izatt JA, Farsiu S. Automatic segmentation of closed-contour features in ophthalmic images using graph theory and dynamic programming. *Biomed Opt Express*. 2012;3:1127–1140.
33. Farsiu S, Chiu SJ, O'Connell RV, et al. Quantitative classification of eyes with and without intermediate age-related macular degeneration using optical coherence tomography. *Ophthalmology*. 2014;121:162–172.
34. Yiu G, Manjunath V, Chiu SJ, Farsiu S, Mahmoud TH. Effect of anti-vascular endothelial growth factor therapy on choroidal thickness in diabetic macular edema. *Am J Ophthalmol*. 2014;158:745–751.e742.
35. Yiu G, Pecen P, Sarin N, et al. Characterization of the choroid-scleral junction and suprachoroidal layer in healthy individuals on enhanced-depth imaging optical coherence tomography. *JAMA Ophthalmol*. 2014;132:174–181.
36. Vuong VS, Moisseiev E, Cunefare D, Farsiu S, Moshiri A, Yiu G. Repeatability of choroidal thickness measurements on enhanced depth imaging optical coherence tomography using different posterior boundaries. *Am J Ophthalmol*. 2016;169:104–112.
37. Willoughby AS, Vuong VS, Cunefare D, et al. Choroidal changes after suprachoroidal injection of triamcinolone acetonide in eyes with macular edema secondary to retinal vein occlusion. *Am J Ophthalmol*. 2018;186:144–151.
38. Wong SS, Vuong VS, Cunefare D, Farsiu S, Moshiri A, Yiu G. Macular fluid reduces reproducibility of choroidal thickness measurements on enhanced depth optical coherence tomography. *Am J Ophthalmol*. 2017;184:108–114.
39. Folgar FA, Yuan EL, Sevilla MB, et al. Drusen volume and retinal pigment epithelium abnormal thinning volume predict 2-year progression of age-related macular degeneration. *Ophthalmology*. 2016;123:39–50 e31.
40. Yiu G, Chiu SJ, Petrou PA, et al. Relationship of central choroidal thickness with age-related macular degeneration status. *Am J Ophthalmol*. 2015;159:617–626.
41. Davis MD, Gangnon RE, Lee LY, et al. The Age-Related Eye Disease Study severity scale for age-related macular degeneration: AREDS Report No. 17. *Arch Ophthalmol*. 2005;123:1484–1498.
42. Chiu SJ, Izatt JA, O'Connell RV, Winter KP, Toth CA, Farsiu S. Validated automatic segmentation of AMD pathology including drusen and geographic atrophy in SD-OCT images. *Invest Ophthalmol Vis Sci*. 2012;53:53–61.
43. Farsiu S, Chiu SJ, O'Connell RV, et al. Quantitative classification of eyes with and without intermediate age-related

Investigative Ophthalmology & Visual Science

macular degeneration using optical coherence tomography. *Ophthalmology*. 2014;121:162–172.
44. Yehoshua Z, Wang F, Rosenfeld PJ, Penha FM, Feuer WJ, Gregori G. Natural history of drusen morphology in age-related macular degeneration using spectral domain optical coherence tomography. *Ophthalmology*. 2011;118:2434–2441.
45. Wu Z, Luu CD, Ayton LN, et al. Optical coherence tomography-defined changes preceding the development of drusen-associated atrophy in age-related macular degeneration. *Ophthalmology*. 2014;121:2415–2422.
46. Ferrara D, Silver RE, Louzada RN, Novais EA, Collins GK, Seddon JM. Optical coherence tomography features preceding the onset of advanced age-related macular degeneration. *Invest Ophthalmol Vis Sci*. 2017;58:3519–3529.
47. Veerappan M, El-Hage-Sleiman AM, Tai V, et al. Optical coherence tomography reflective drusen substructures predict progression to geographic atrophy in age-related macular degeneration. *Ophthalmology*. 2016;123:2554–2570.
48. Ouyang Y, Heussen FM, Hariri A, Keane PA, Sadda SR. Optical coherence tomography-based observation of the natural history of drusenoid lesion in eyes with dry age-related macular degeneration. *Ophthalmology*. 2013;120:2656–2665.
49. Oishi A, Thiele S, Nadal J, et al. Prevalence, natural course, and prognostic role of refractile drusen in age-related macular degeneration. *Invest Ophthalmol Vis Sci*. 2017;58:2198–2206.
50. Querques G, Merle BM, Pumariega NM, et al. Dynamic drusen remodelling in participants of the Nutritional AMD Treatment-2 (NAT-2) randomized trial. *PLoS One*. 2016;11:e0149219.
51. Querques G, Georges A, Ben Moussa N, Sterkers M, Souied EH. Appearance of regressing drusen on optical coherence tomography in age-related macular degeneration. *Ophthalmology*. 2014;121:173–179.
52. Sarks S, Cherepanoff S, Killingsworth M, Sarks J. Relationship of basal laminar deposit and membranous debris to the clinical presentation of early age-related macular degeneration. *Invest Ophthalmol Vis Sci*. 2007;48:968–977.
53. Sarks JP, Sarks SH, Killingsworth MC. Evolution of soft drusen in age-related macular degeneration. *Eye (Lond)*. 1994;8(pt 3):269–283.
54. Sarks SH. Ageing and degeneration in the macular region: a clinico-pathological study. *Br J Ophthalmol*. 1976;60:324–341.
55. Sarks SH, Arnold JJ, Killingsworth MC, Sarks JP. Early drusen formation in the normal and aging eye and their relation to age related maculopathy: a clinicopathological study. *Br J Ophthalmol*. 1999;83:358–368.
56. Ruberti JW, Curcio CA, Millican CL, Menco BP, Huang JD, Johnson M. Quick-freeze/deep-etch visualization of age-related lipid accumulation in Bruch's membrane. *Invest Ophthalmol Vis Sci*. 2003;44:1753–1759.
57. Li CM, Chung BH, Presley JB, et al. Lipoprotein-like particles and cholesteryl esters in human Bruch's membrane: initial characterization. *Invest Ophthalmol Vis Sci*. 2005;46:2576–2586.
58. Curcio CA. Soft drusen in age-related macular degeneration: biology and targeting via the oil spill strategies. *Invest Ophthalmol Vis Sci*. 2018;59:AMD160–AMD181.
59. Curcio CA, Millican CL. Basal linear deposit and large drusen are specific for early age-related maculopathy. *Arch Ophthalmol*. 1999;117:329–339.
60. Curcio CA, Presley JB, Malek G, Medeiros NE, Avery DV, Kruth HS. Esterified and unesterified cholesterol in drusen and basal deposits of eyes with age-related maculopathy. *Exp Eye Res*. 2005;81:731–741.
61. Curcio CA, Presley JB, Millican CL, Medeiros NE. Basal deposits and drusen in eyes with age-related maculopathy: evidence for solid lipid particles. *Exp Eye Res*. 2005;80:761–775.
62. Balaratnasingam C, Messinger JD, Sloan KR, Yannuzzi LA, Freund KB, Curcio CA. Histologic and optical coherence tomographic correlates in drusenoid pigment epithelium detachment in age-related macular degeneration. *Ophthalmology*. 2017;124:644–656.
63. Suzuki M, Curcio CA, Mullins RF, Spaide RF. Refractile drusen: clinical imaging and candidate histology. *Retina*. 2015;35:859–865.
64. Thompson RB, Reffatto V, Bundy JG, et al. Identification of hydroxyapatite spherules provides new insight into subretinal pigment epithelial deposit formation in the aging eye. *Proc Natl Acad Sci USA*. 2015;112:1565–1570.
65. Curcio CA, Zanzottera EC, Ach T, Balaratnasingam C, Freund KB. Activated retinal pigment epithelium, an optical coherence tomography biomarker for progression in age-related macular degeneration. *Invest Ophthalmol Vis Sci*. 2017;58:BIO211–BIO226.
66. Mullins RF, Johnson MN, Faidley EA, Skeie JM, Huang J. Choriocapillaris vascular dropout related to density of drusen in human eyes with early age-related macular degeneration. *Invest Ophthalmol Vis Sci*. 2011;52:1606–1612.
67. Curcio CA, Millican CL, Bailey T, Kruth HS. Accumulation of cholesterol with age in human Bruch's membrane. *Invest Ophthalmol Vis Sci*. 2001;42:265–274.
68. Killingsworth MC. Age-related components of Bruch's membrane in the human eye. *Graefes Arch Clin Exp Ophthalmol*. 1987;225:406–412.
69. Feeney-Burns L, Hilderbrand ES, Eldridge S. Aging human RPE: morphometric analysis of macular, equatorial, and peripheral cells. *Invest Ophthalmol Vis Sci*. 1984;25:195–200.
70. Lambert V, Lecomte J, Hansen S, et al. Laser-induced choroidal neovascularization model to study age-related macular degeneration in mice. *Nat Protoc*. 2013;8:2197–2211.
71. Moshiri A, Chen R, Kim S, et al. A nonhuman primate model of inherited retinal disease. *J Clin Invest*. 2019;129:863–874.
72. Wang L, Li CM, Rudolf M, et al. Lipoprotein particles of intraocular origin in human Bruch membrane: an unusual lipid profile. *Invest Ophthalmol Vis Sci*. 2009;50:870–877.
73. Bretillon L, Thuret G, Gregoire S, et al. Lipid and fatty acid profile of the retina, retinal pigment epithelium/choroid, and the lacrimal gland, and associations with adipose tissue fatty acids in human subjects. *Exp Eye Res*. 2008;87:521–528.
74. McGill TJ, Renner LM, Neuringer M. Elevated fundus autofluorescence in monkeys deficient in lutein, zeaxanthin, and omega-3 fatty acids. *Invest Ophthalmol Vis Sci*. 2016;57:1361–1369.
75. Guymer RH, Baird PN, Varsamidis M, et al. Proof of concept, randomized, placebo-controlled study of the effect of simvastatin on the course of age-related macular degeneration. *PLoS One*. 2013;8:e83759.
76. Vavvas DG, Daniels AB, Kapsala ZG, et al. Regression of some high-risk features of age-related macular degeneration (AMD) in patients receiving intensive statin treatment. *EBioMedicine*. 2016;5:198–203.
77. Tan ACS, Pilgrim MG, Fearn S, et al. Calcified nodules in retinal drusen are associated with disease progression in age-related macular degeneration. *Sci Transl Med*. 2018;10:eaat4544.
78. Curcio CA, Messinger JD, Sloan KR, McGwin G, Medeiros NE, Spaide RF. Subretinal drusenoid deposits in non-neovascular age-related macular degeneration: morphology,

Investigative Ophthalmology & Visual Science

prevalence, topography, and biogenesis model. *Retina*. 2013;33:265–276.

79. Yehoshua Z, de Amorim Garcia Filho CA, Nunes RP, et al. Systemic complement inhibition with eculizumab for geographic atrophy in age-related macular degeneration: the COMPLETE study. *Ophthalmology*. 2014;121:693–701.
80. Schaal KB, Rosenfeld PJ, Gregori G, Yehoshua Z, Feuer WJ. Anatomic clinical trial endpoints for nonexudative age-related macular degeneration. *Ophthalmology*. 2016;123:1060–1079.
81. Copland DA, Theodoropoulou S, Liu J, Dick AD. A perspective of AMD through the eyes of immunology. *Invest Ophthalmol Vis Sci*. 2018;59:AMD83–AMD92.
82. Yiu G, Vuong VS, Tran S, et al. Vascular response to sildenafil citrate in aging and age-related macular degeneration. *Sci Rep*. 2019;9:5049.
83. Snyder K, Yazdanyar A, Mahajan A, Yiu G. Association between the cilioretinal artery and choroidal neovascularization in age-related macular degeneration: a secondary analysis from the Age-Related Eye Disease Study. *JAMA Ophthalmol*. 2018;136:1008–1014.

Investigative Ophthalmology & Visual Science